Measurement of dilepton production from photon fusion processes in Pb+Pb UPC with the ATLAS detector

I. Grabowska-Bold (for the ATLAS Collaboration)
Faculty of Physics and Applied Computer Science, AGH University of Krakow.
Al. Mickiewicza 30, 30-059 Kraków, Poland

Relativistic heavy-ion beams at the LHC are accompanied by a large flux of equivalent photons, leading to multiple photon-induced processes. This report presents a series of measurements of dilepton production from photon fusion performed by the ATLAS Collaboration. Recent measurements of exclusive dielectron production in ultra-peripheral collisions (UPC) are presented. These processes provide strong constraints on the nuclear photon flux and its dependence on the impact parameter and photon energy. Comparisons of the measured cross sections to QED predictions from the STARlight and SuperChic models are also presented. Tau-pair production measurements can constrain the tau lepton's anomalous magnetic dipole moment (g-2), and a recent ATLAS measurement using muonic decays of tau leptons in association with electrons and tracks provides one of the most stringent limits available to date. Furthermore, measurements of muon pairs produced via two-photon scattering processes in hadronic (i.e. non-UPC) Pb+Pb collisions are discussed. These non-UPC measurements provide a novel test of strong-field QED and may be a potentially sensitive electromagnetic probe of the quark-gluon plasma. These measurements include the dependence of the cross section and angular correlation on the mean-p_{T} of the dimuon pair, the rapidity separation between the muons, and the angle of the pair relative to the second-order event-plane, all measured differentially as a function of the Pb+Pb collision centrality.

Keywords: ultra-peripheral collisions, photon-induced processes, exclusive production of lepton pairs, tau anomalous magnetic moment, non-UPC dimuons

ATL-PHYS-PROC-2024-023
26 March 2024

1 Introduction

Heavy-ion collisions at ultra-relativistic energies are typically examined in processes in which nuclear beams interact hadronically at impact parameters less than twice the nuclear radius. In the overlap region of two colliding nuclei a dense quark–gluon plasma is expected to be produced. On the other hand, the strong electromagnetic (EM) fields associated with the nuclei can also lead to interactions in ultra-peripheral collisions (UPC), events with impact parameters well beyond twice the nuclear radius, where any contributions from strong processes are suppressed.

At high energies of the Large Hadron Collider (LHC), UPC can induce a wide variety of exclusive final states – dileptons, dijets, and diphotons being the most commonly studied – for which no other activity in the detectors is observed, except for nucleons emitted at very small angles relative to the beam direction. The photons are also characterized by small transverse momenta, such that high-energy decay products in these exclusive final states are almost perfectly balanced in the transverse direction. UPC processes have also been proposed to be utilized as a competitive tool to search for beyond Standard Model (BSM) physics [1].

In this report the most recent results on photon-photon ($\gamma\gamma$) induced processes in UPC physics from the ATLAS experiment [2] are reviewed. Furthermore, a measurement of the $\gamma\gamma \to \mu^+\mu^-$ process occurring simultaneously to hadronic Pb+Pb collisions is studied. Prospects for the 2023 Pb+Pb data are also discussed.

2 Exclusive dimuon and dielectron production

ATLAS measured exclusive $\gamma\gamma \to \mu^+\mu^-$ production [3] in UPC Pb+Pb collisions at $\sqrt{s_{\rm NN}} = 5.02$ TeV collisions in the data set with an integrated luminosity of 0.48 nb^{-1}. The fiducial region of the measurement is defined by single muon $p_{\rm T} > 4$ GeV and $|\eta| < 2.4$. Furthermore, requirements on invariant mass of the dimuon system, $m_{\mu\mu} > 10$ GeV, and its transverse momentum, $p_{\rm T}^{\mu\mu} < 2$ GeV, are imposed. The event selection allows exactly two opposite-charge muons per event with no other activity in the detector. It results in about 12k event candidates from the $\gamma\gamma \to \mu^+\mu^-$ process. After the evaluation and subtraction of dissociative background, which amounts to 3%, differential cross sections are measured in $m_{\mu\mu}$, dimuon rapidity $y_{\mu\mu}$, scattering angle in the dimuon rest frame $\cos\theta^*$, initial-photon momenta $k_{\rm min}$, $k_{\rm max}$ and acoplanarity, $\alpha = 1 - |\Delta\phi|/\pi$ as well as the integrated cross section. The latter quantifies how two muons are aligned in the azimuthal angle.

The left panel of Figure 1 presents differential cross sections for exclusive $\gamma\gamma \to \mu^+\mu^-$ production as a function of α. STARLIGHT [4] fails in describing a tail of this differential cross section. For $\alpha > 5 \times 10^{-3}$

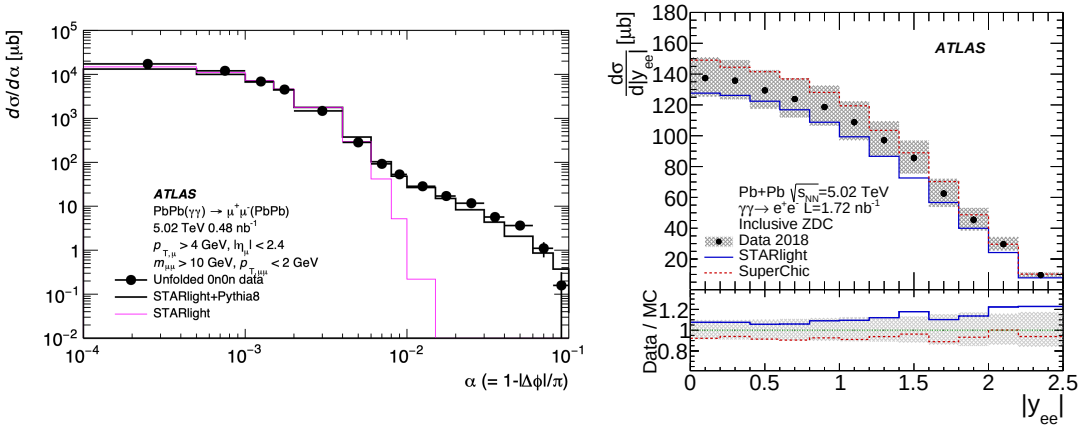

Figure 1 – (Left) Differential cross section as a function of acoplanarity (right) for exclusive $\gamma\gamma \to \mu^+\mu^-$ production in UPC Pb+Pb collisions [3]. Data points are compared with predictions from STARLIGHT or STARLIGHT+PYTHIA to account for the FSR contribution. (Right) Differential cross section as a function of $|y_{ee}|$ for exclusive $\gamma\gamma \to e^+e^-$ production in UPC Pb+Pb collisions [6]. In the bottom panel, data-to-prediction ratio is shown for STARLIGHT and SUPERCHIC.

an expected contribution of signal events is suppressed and the excess of data is visible. It is caused by a contribution from the final state radiation (FSR) which is not accounted for in the STARLIGHT calculation. A better description of the full α distribution is obtained by interfacing STARLIGHT with PYTHIA which accounts for the FSR contribution. This result demonstrates need for FSR modeling to get a good description of the data by the calculation for exclusive dilepton production.

A measurement of exclusive $\gamma\gamma \to e^+e^-$ production was performed [6] by ATLAS in the Pb+Pb data set with an integrated luminosity of 1.72 nb^{-1}. The fiducial region of the measurement is defined by single electron $p_{\rm T} > 2.5$ GeV and $|\eta| < 2.5$. Furthermore, requirements on invariant mass of the dielectron system, $m_{ee} > 5$ GeV, and its transverse momentum, $p_{\rm T}^{ee} < 2$ GeV, are imposed. The event selection requires exactly two opposite-charge electrons per event and no other activity in the detector. In comparison to the $\gamma\gamma \to \mu^+\mu^-$ measurement, the dielectron analysis features three times larger statistics, the extended fiducial coverage at low electron $p_{\rm T}$ and m_{ee}, and advancement in the background evaluation techniques.

The right panel of Figure 1 shows differential cross sections for exclusive $\gamma\gamma \to e^+e^-$ production as a function of $|y_{ee}|$, where y_{ee} stands for rapidity of the dielectron system. The data is corrected to the Born level i.e. before the FSR. The measurement precision is dominated by systematic uncertainties. The data is compared with two Monte Carlo (MC) predictions for the $\gamma\gamma \to e^+e^-$ process: STARLIGHT v3.13 and SUPERCHIC v3.05 [5], which are systematically about 10% lower and higher than the data, respectively. SUPERCHIC tends to better describe the shape of the distribution.

3 Forward neutron activity in $\gamma\gamma \to \ell^+\ell^-$ events

An inclusive sample of $\gamma\gamma \to \ell^+\ell^-$ events with $\ell^\pm = \mu^\pm, e^\pm$ can be inspected using information from the Zero Degree Calorimeters (ZDC) which are located in the forward region ± 140 m away from the ATLAS interaction point (IP). The ZDC detectors are designed to detect neutral particles originating from IP. In particular in hadronic Pb+Pb collisions they detect spectator neutrons. On the other hand, in UPC events the probability of exchanging one or more photons between the two incoming ions is sizable. These additional photons may dissociate one or both nuclei and cause emission of single neutrons in ZDC. Because of the radial dependence of the photon flux [7], the presence of these additional photons can preferentially select certain impact parameter ranges, and so can influence the photon spectrum of the other photons.

ATLAS measured forward neutron activity in exclusive $\gamma\gamma \to \mu^+\mu^-$ [3] and $\gamma\gamma \to e^+e^-$ [6] processes. In both cases, all $\gamma\gamma \to \ell^+\ell^-$ event candidates are divided into three categories.

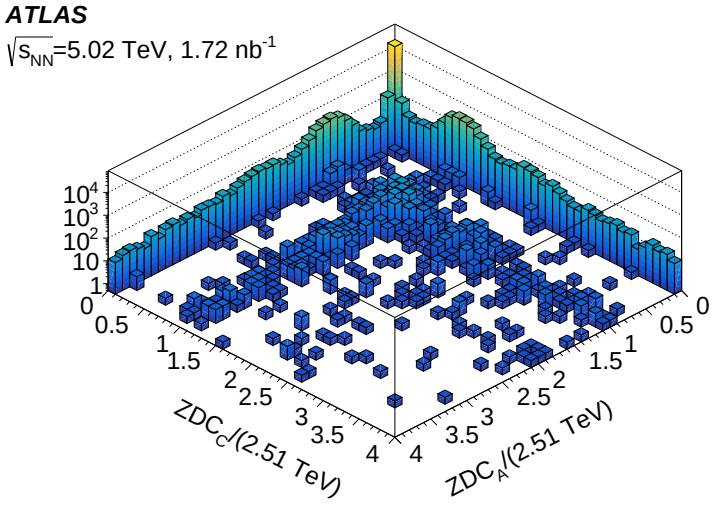

Figure 2 – Correlation of energy deposited in each of the ZDC arms, normalized to the per-nucleon beam energy, in a sample of $\gamma\gamma \to e^+e^-$ events [6].

Figure 2 shows the correlation of energies normalized to the per-nucleon beam energy in both ZDC sides. It illustrates the three primary topologies available for these events: 1) the most probable configuration is no activity in either ZDC ("0n0n"), 2) the next mostly likely configuration is observing one or more forward neutrons in one ZDC, and none in the other ("Xn0n"), and 3) finally, the rarest configuration is observing one or more forward neutrons in both ZDC arms ("XnXn").

After subtracting the dissociative background contribution and accounting for simultaneous EM interactions in the same bunch crossing, fractions of events falling into each category are measured.

The left panel of Figure 3 shows corrected fractions of events in the 0n0n category measured in $\gamma\gamma \to e^+e^-$ data as a function of m_{ee} in three bins of $|y_{ee}|$. These fractions drop from about 80% at low m_{ee} to 60% at high m_{ee} and $|y_{ee}| < 0.8$, and in general are larger for higher $|y_{ee}|$ values. These observations are consistent with the conclusions for forward neutron activity measured in the $\gamma\gamma \to \mu^+\mu^-$ process [3].

The right panel of Figure 3 presents the differential cross section as a function of $|y_{ee}|$ for the 0n0n category of the $\gamma\gamma \to e^+e^-$ process. It is compared with the MC predictions from STARLIGHT and SUPERCHIC. Both simulated samples were produced inclusively and reweighted to the 0n0n category using the measured fractions. Each theory prediction is represented by two curves reflecting the systematic variations of the measured 0n0n fractions. STARLIGHT can also generate a prediction conditional on the presence of neutron emission in one or both directions. These dedicated predictions from STARLIGHT for the 0n0n category are shown in the same plots. That prediction agrees well with the shape of the inclusive STARLIGHT calculation corrected for the measured 0n0n fractions, but is systematically lower by 2%–3% for $|y_{ee}| < 1.4$. The general conclusions from this comparison between MC predictions and data are consistent with the inclusive case presented in Section 2.

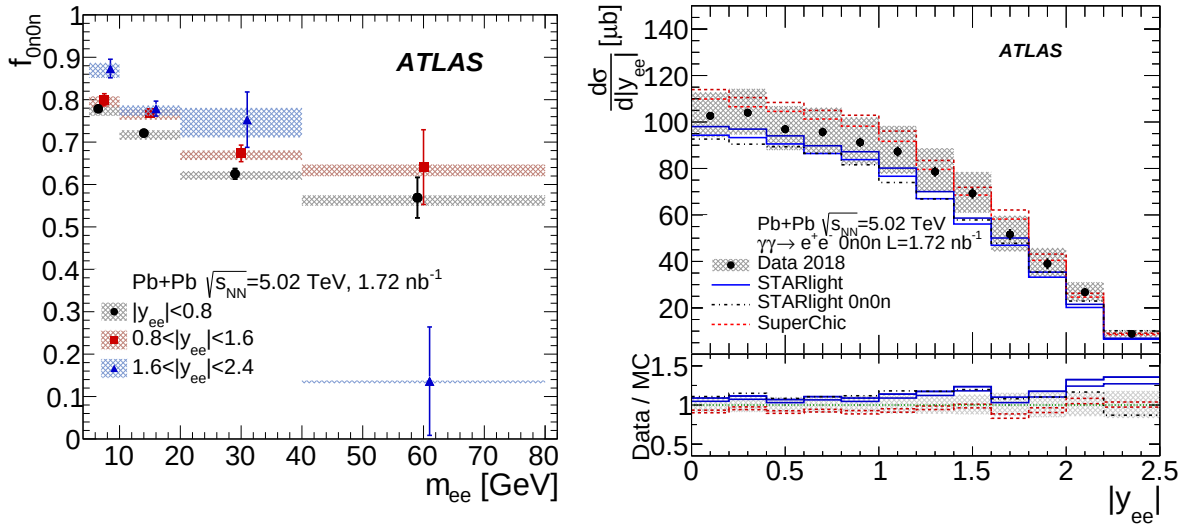

Figure 3 – (Left) Fractions of events in the 0n0n category evaluated from $\gamma\gamma \to e^+e^-$ data in three ranges of the dielectron rapidity, $|y_{ee}|$, corrected for the presence of additional neutrons [6]. Error bars represent statistical uncertainties, while shaded boxes represent systematic uncertainties. Points for $|y_{ee}| < 0.8$ and $1.6 < |y_{ee}| < 2.4$ are displaced horizontally for better visibility. (Right) Differential cross section measured for the 0n0n category for exclusive dielectron production as a function of $|y_{ee}|$ [6]. The cross section is compared with MC predictions from STARLIGHT (solid blue) and SUPERCHIC v3.05 (dashed red), each represented by two lines reflecting systematic variations. Also, a dedicated prediction from STARLIGHT for the 0n0n category (dashed-dotted black) is shown. The bottom panels show the ratios of data to predictions. The shaded area represents the total uncertainty of the data, excluding the 2% luminosity uncertainty.

4 Exclusive $\gamma\gamma \to \tau^+\tau^-$ production and tau anomalous magnetic moment

The ATLAS Collaboration made the observation of exclusive $\gamma\gamma \to \tau^+\tau^-$ production [8] in 2018 Pb+Pb collisions with an integrated luminosity of 1.44 nb^{-1}. Selected events contain one muon from a τ-lepton decay, an electron or charged-particle track(s) from the other τ-lepton decay, little additional central-detector activity, and no forward neutrons (0n0n category). After applying the full event selection, a total of 656 data events are observed in three signal regions (SR) in which the analysis is conducted. Figure 4 presents pre-fit control plots for muon-track invariant mass in the SR with one muon and one track (labeled μ1T-SR), three-track invariant mass in the SR with one muon and three tracks (labeled μ3T-SR), and muon-electron invariant mass in the SR with one muon and one electron (labeled μe-SR). A total of 532, 85, and 39 data events are observed in the μ1T-SR, μ3T-SR, and μe-SR, respectively. The most dominant background contributions in the SRs originate from exclusive $\gamma\gamma \to \mu^+\mu^-$ followed by FSR and dissociative photo-nuclear processes. Overall background is expected to contribute 84 ± 19, 9 ± 3, and 2.8 ± 0.7 events in the μ1T-SR, μ3T-SR, and μe-SR, respectively.

The $\gamma\gamma \to \tau^+\tau^-$ process is observed with a significance exceeding 5 standard deviations, and a signal strength of $\mu_{\tau\tau} = 1.03^{+0.06}_{-0.05}$ assuming the Standard Model value for the anomalous magnetic moment of the τ lepton, a_τ. The left panel of Figure 5 shows $\mu_{\tau\tau}$ extracted from the fit, based on the individual SRs. The combined $\mu_{\tau\tau}$ is also shown which is in agreement with the prediction from the Standard Model.

The measurement of $\gamma\gamma \to \tau^+\tau^-$ production from ATLAS provides also constraints on a_τ [8]. To measure a_τ, a profile-likelihood fit to the muon p_{T} distribution is performed in the three SRs with a_τ being the only free parameter. Also a control region with events from the $\gamma\gamma \to \mu^+\mu^-$ process is used in the fit to constrain initial-photon fluxes. The right panel of Figure 5 depicts the a_τ measurement alongside previous results obtained at LEP. The precision of this measurement is similar to the most precise single-experiment measurement by the DELPHI Collaboration [9].

5 Non-UPC dimuon production

Dimuon production induced by $\gamma\gamma$ fusion was also measured by ATLAS using non-UPC Pb+Pb collisions [10] spanning all centralities with an integrated luminosity of 1.94 nb^{-1}. The $\gamma\gamma \to \mu^+\mu^-$ pairs are identified using selections on pair momentum asymmetry, $A = (|p_{\mathrm{T},1} - p_{\mathrm{T},2}|/(p_{\mathrm{T},1} + p_{\mathrm{T},2}))$, and acopla-

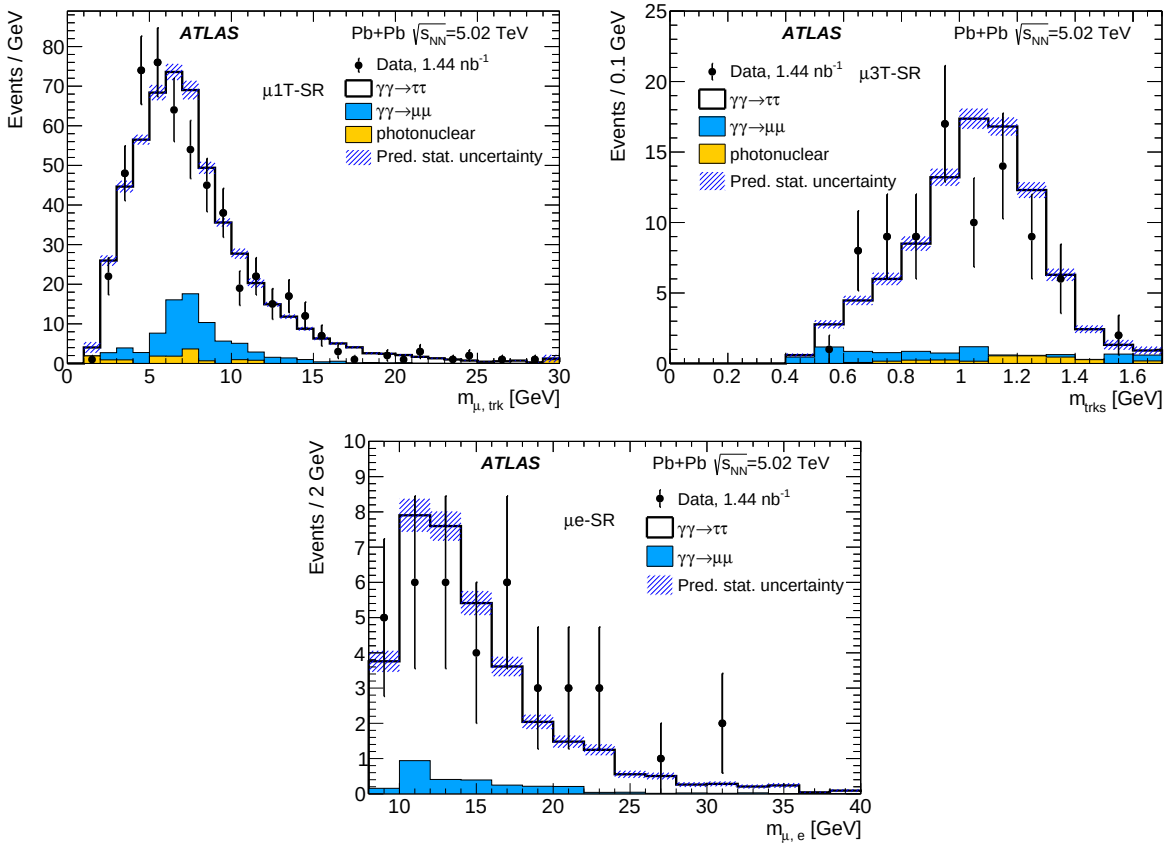

Figure 4 – Pre-fit control plots for (top-left) muon-track invariant mass in the μ1T-SR, (top-right) 3-track invariant mass in the μ3T-SR, (bottom) muon–electron invariant mass in the μe-SR [8]. Statistical uncertainties on the predictions are shown as hatched bands.

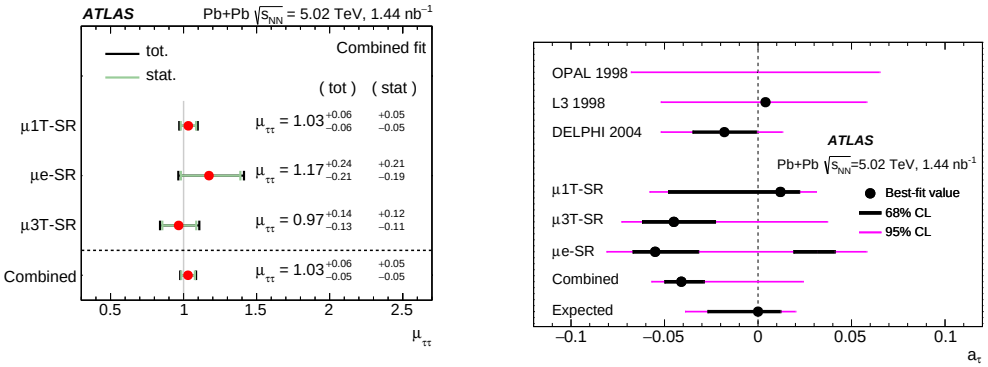

Figure 5 – (Left) Best-fit values of the signal strength parameter, $\mu_{\tau\tau}$, under the Standard Model a_τ value assumption, extracted from the fit based on the individual SRs [8]. (Right) Anomalous magnetic moment of tau a_τ from fits to individual SRs, and from the combined fit [8]. These are compared with existing measurements from the OPAL, L3 and DELPHI experiments at LEP.

narity of the dimuon system, α. Backgrounds, dominated by heavy-flavor decays, are evaluated using template fits to the distribution of muon-pair transverse impact parameter.

The STARLIGHT model, which was recently augmented to allow evaluation of cross sections for $\gamma\gamma \to \mu^+\mu^-$ production within restricted impact parameter intervals, is found to substantially underestimate the measured cross sections. Measurements of α and the associated transverse momentum scale, $k_\perp = \pi\alpha\bar{p_{\rm T}}$, distributions ($\bar{p_{\rm T}}$ stands for an average $p_{\rm T}$ of the two muons) confirm a significant centrality dependence in mean, RMS and standard deviations which are shown for α in Figure 6. The moments calculated for the initial-state QED [11] and PWF [12] predictions are in excellent agreement with each other except for the most central collisions where the QED results are slightly higher. Both calculations show systematic differences from the data in all centrality intervals including more peripheral collisions. Especially in the 60–70% and 70–80% intervals they are significant.

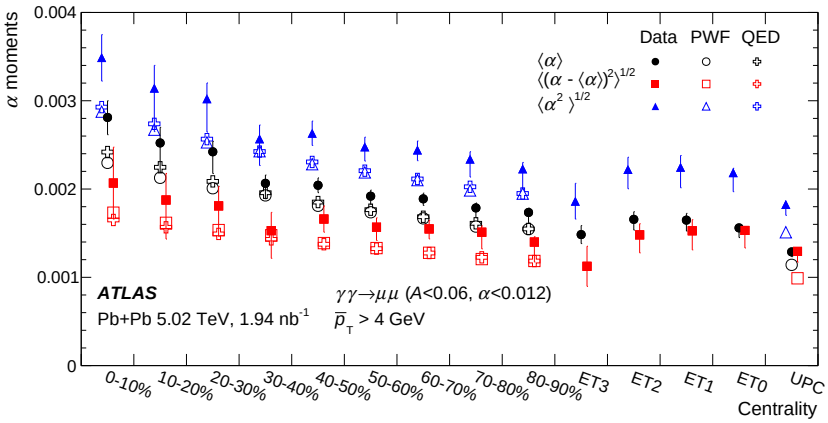

Figure 6 – Moments of the $\gamma\gamma \to \mu^+\mu^-$ acoplanarity distributions as a function of centrality compared with the QED and PWF predictions [10]. The error bars on the data points indicate combined statistical and systematic uncertainties.

With the improved statistical precision of this measurement, an additional depletion is observed in the α and $k_\perp$ distributions near zero values of the corresponding quantities. In more peripheral collisions, both calculations show weaker suppression near $\alpha = 0$ than is observed in the data. This is demonstrated in Figure 7 which shows the evolution of the α distribution as a function of centrality.

Moreover, the predicted trends associated with effects of magnetic fields on the dimuons are not observed in the ATLAS data.

6 Prospects for 2023 Pb+Pb measurements

In fall of 2023, a first high-luminosity data-taking campaign for heavy ions took place as part of Run-3 operations. Pb+Pb collisions were provided at the record center-of-mass energy of 5.36 TeV per nucleon pair. In preparation to the data-taking new triggering techniques were developed and optimized to provide better performance. Also the offline reconstruction for some objects was tuned. Last but not least the ZDC detectors were refurbished what resulted in a new functionality.

The left panel of Figure 8 shows a comparison of the average $p_{\rm T}$ for electrons from the $\gamma\gamma \to e^+e^-$ process between 2023 (markers) and 2018 (solid histogram) Pb+Pb data from UPC. The excess of electrons in the region of $2 < p_{\rm T} < 5$ GeV results from the dedicated electron/photon reconstruction optimization for Run 3 and also dedicated trigger developments [14]. This improvement will extend future measurements involving electrons in UPC to cover this new kinematic regime. The reduction of systematic uncertainties originating from the limited statistics of electron/photon candidates in the Run-2 data is also anticipated. Improvements to photon reconstruction at low-$p_{\rm T}$ will open an opportunity for a new series of measurements involving photons from light-by-light scattering [16].

The right panel of Figure 8 depicts two-track invariant mass in the J/ψ window for events selected online using a novel approach with the Transition Radiation Tracker (TRT) trigger [15]. A clear excess of J/ψ event candidates can be identified at $m_{\rm 2trk} = 3.1$ GeV. Also large statistics of dimuon candidates contributing to the continuum region is visible. This development paves a way for dimuon measurements with low $p_{\rm T}$ muons in UPC Pb+Pb by ATLAS for the first time.

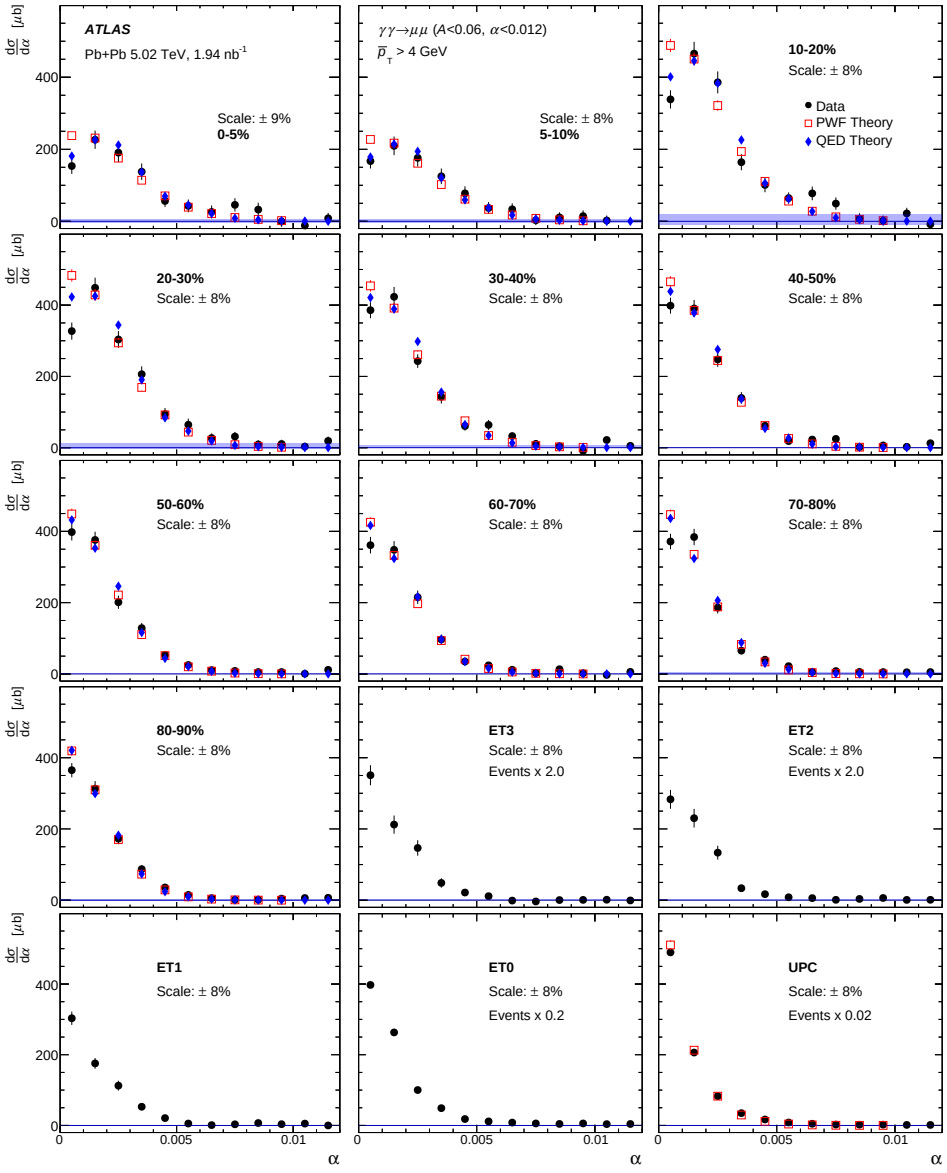

Figure 7 – Differential cross sections as a function of α for $\gamma\gamma \to \mu^+\mu^-$ pairs [10]. Each panel represents a different centrality interval, with the last panel representing the UPC events. The error bars indicate combined statistical and systematic uncertainties, excluding the background subtraction uncertainties, which are indicated by a shaded band at $d\sigma/d\alpha = 0$, and overall normalization uncertainties, which are quoted on each panel as "Scale". Also shown are the results of the QED and PWF theoretical calculations.

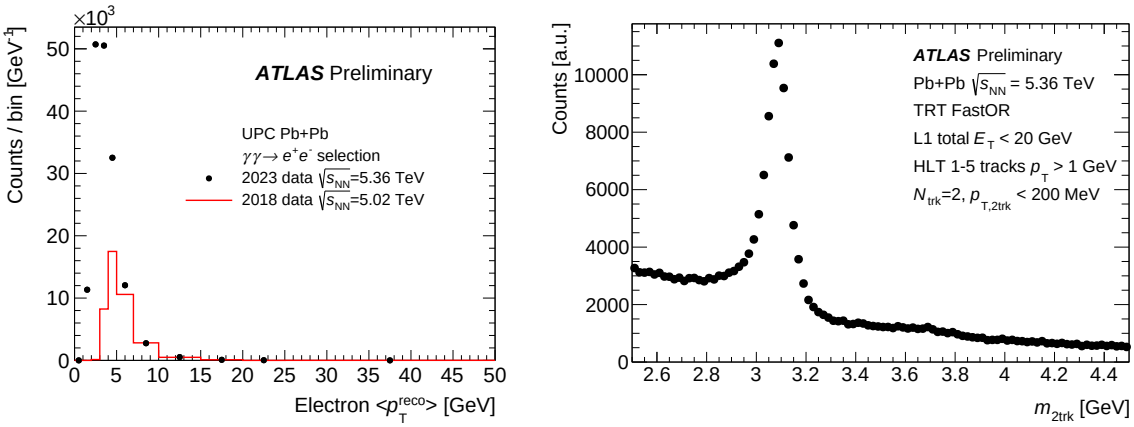

Figure 8 – (Left) Comparison of the average electron p_{T} between 2023 (markers) and 2018 (solid histogram) Pb+Pb data from UPC [13]. (Right) Two-track invariant mass in the J/ψ region for events selected by the level-1 TRT trigger.

7 Summary and outlook

In this report, the latest results for $\gamma\gamma$ fusion processes from the ATLAS Collaboration were discussed. The UPC physics program focused on precise measurements of exclusive $\gamma\gamma \to \mu^+\mu^-$ and $\gamma\gamma \to e^+e^-$ production including also forward neutron emission. Thanks to a large integrated luminosity of Pb+Pb collisions collected by ATLAS, low-rate processes such as $\gamma\gamma \to \tau^+\tau^-$ could be measured at the LHC for the first time. Also UPC proved to be a competitive tool for BSM searches. In particular, they provided constraints on τ anomalous magnetic moment with the precision comparable to the best world-limits from the LEP experiments. The latest precision results for $\gamma\gamma \to \mu^+\mu^-$ measured in non-UPC Pb+Pb collisions in all centralities revealed new features and made progress on the interpretation using the latest initial-state calculations. With a new sample of Pb+Pb data collected at the record center-of-mass energy of 5.36 TeV with about 1.7 nb^{-1} at the end of 2023, the ATLAS UPC physics program has a bright future.

Acknowledgments

This work was partly supported by the National Science Center of Poland under grant number UMO-2020/37/B/ST2/01043 and by PL-GRID infrastructure.

References

1. D. d'Enterria et al., J. Phys. G: Nucl. Part. Phys. **50**, 050501 (2023), doi:10.1088/1361-6471/
2. ATLAS Collaboration, JINST **3**, S08003 (2008), doi:10.1088/1748-0221/3/08/S08003
3. ATLAS Collaboration, Phys. Rev. **C 104**, 024906 (2021), https://doi.org/10.1103/PhysRevC.104.024906
4. S.R. Klein et al., Comp. Phys. Comm. **212**, 258 (2017), https://doi.org/10.1016/j.cpc.2016.10.016
5. L. A. Harland-Lang et al., Eur. Phys. J. C **76**, 1-9 (2016), https://doi.org/10.1140/epjc/s10052-015-3832-8
6. ATLAS Collaboration, J. High Energy Phys. **06**, 182 (2023), https://doi.org/10.1007/JHEP06(2023)182
7. S.R. Klein, P. Steinberg, Ann. Rev. Nucl. Part. Sci. **70**, 323-354 (2020), https://doi.org/10.1146/annurev-nucl-030320-033923
8. ATLAS Collaboration, Phys. Rev. Lett. **131**, 151802 (2023), https://doi.org/10.1103/PhysRevLett.131.151802
9. DELPHI Collaboration, Eur. Phys. J. **C 35**, 159 (2004), doi:10.1140/epjc/s2004-01852-y
10. ATLAS Collaboration, Phys. Rev. **C 107**, 054907 (2023), https://doi.org/10.1103/PhysRevC.107.054907

11. S. Klein, A. H. Mueller, B.-W. Xiao, and F. Yuan, Phys. Rev. **D 102**, 094013 (2020), https://doi.org/10.1103/PhysRevD.102.094013
12. W. Zha, J. D. Brandenburg, Z. Tang, and Z. Xu, Phys. Lett. **B 800**, 135089 (2020), https://doi.org/10.1016/j.physletb.2019.135089
13. ATLAS Collaboration, https://atlas.web.cern.ch/Atlas/GROUPS/PHYSICS/PLOTS/HION-2023-001/
14. Karolina Domijan (for the ATLAS Collaboration), https://cds.cern.ch/record/2881824, https://doi.org/10.22323/1.450.0265
15. Pawel Rybczynski (for the ATLAS Collaboration), https://cds.cern.ch/record/2891399
16. ATLAS Collaboration, J. High Energy Phys. **03**, 243 (2021), https://doi.org/10.1007/JHEP03(2021)243